Journal of Magnetic Resonance 198 (2009) 215–221

Contents lists available at ScienceDirect

Journal of Magnetic Resonance

journal homepage: www.elsevier.com/locate/jmr

TNT detection with ^{14}N NQR: Multipulse sequences and matched filter

Alan Gregorovič *, Tomaž Apih

Institute Jožef Stefan, Solid State Physics, Jamova 39, 1000 Ljubljana, Slovenia

ARTICLE INFO

Article history:
Received 24 December 2008
Revised 23 February 2009
Available online 28 February 2009

Keywords:
Nuclear quadrupole resonance
NQR
Trinitrotoluene
TNT
Multipulse sequences
Spin lock

ABSTRACT

Nuclear quadrupole resonance (NQR) has a distinct potential to verify the presence of nitrogen bearing substances based on the unequivocal signatures of their spectra. Therefore, this technique is especially suitable for remote detection of illicit substances and explosives. Unfortunately, the inherent signal-to-noise of the most abundant explosive trinitrotoluene (TNT) is very low. Here we present an NQR method with improved sensitivity for estimation of the probability of TNT presence in the investigated object. The method consists of a spin-lock spin-echo (SLSE) multipulse sequence for signal excitation and a time domain matched filter for signal detection. We find that the signal-to-noise increases by shortening the pulse spacings, even though this means a decrease in spectral resolution. In our case, the decrease of the pulse spacings from the typical 2 ms to 540 μs resulted in an increase of the signal-to-noise by 14 dB. A theory describing this enhancement is presented and compared to experimental results on TNT. Issues related to temperature and polymorphism variations are also discussed.

1. Introduction

The remote detection of trinitrotoluene (TNT) with ^{14}N nuclear quadrupole resonance (NQR) has a huge potential [1,2], but it has not reached widespread use primarily because of TNT inherent low signal-to-noise ratio (S/N). The later has two principal origins: (i) a low resonance frequency $\sim$ 850 kHz and (ii) a long spin-lattice relaxation time of several seconds preventing fast averaging. The S/N is further reduced by a very low filling factor of a typical remote detection coil. In addition, there is significant RF interference in this frequency band from AM radio stations, electronic equipment, power lines, etc... Nevertheless, NQR signal is characteristic of a solid material, as shown in Fig. 1, and provides means of a reliable material identification with very few errors. This is a big advantage of NQR in respect of competitive techniques used for explosive detection, since many of them are indirect and detect only features of the explosive device, but not the explosive itself. Among these are also the two "workhorses" of landmine detection, the prodder and the metal detector. Both generate a big rate of false alarms and the search for a better technique is an utmost priority.

The low TNT ^{14}N NQR S/N has been dealt with in several ways. One of the first approaches to increase the S/N was by modifying the pulse sequence. Typically, the TNT ^{14}N NQR signal is acquired by detecting its spin echo. If instead we average several echoes obtained with a CPMG type multipulse sequence, an increase of S/N for $\sim$ 6 dB can be obtained with practically no time penalty. Here the increase of S/N is determined by the ratio of the spin–spin relaxation time T_2 and signal decay time T_2^*. The S/N can be increased by much more, $\sim$ 20 dB, with the spin-lock spin-echo (SLSE) multipulse sequence [3,4]. Here the inter-pulse distances are shorter than T_2^* and the so called "spin-lock" effect is created. The magnetization is locked in the effective magnetic field for times up to $3T_{2\mathrm{eff}} \sim 150$ ms. However, the later technique results in a reduced spectral resolution. A further attempt involved the use of double resonance techniques [5,6], by indirectly detecting ^{14}N via its influence on ^{1}H. This technique gives a really big S/N enhancement but requires a sophisticated apparatus, with a very homogeneous magnetic field and fast field switching capabilities, which are too demanding for remote detection. Recently, a modification of the above technique which removes the requirement of a homogeneous magnetic field [7,8] was demonstrated for TNT with cross-polarization from ^{1}H to ^{14}N. Here ^{1}H magnetization acquired in the magnetic field is transferred to ^{14}N nuclei, whose NQR signal is subsequently observed. Only the magnetic field average value determines the signal enhancement with typical values of 50 for the laboratory conditions, while practical values for remote detection are around 10. Other techniques which modestly improve the S/N include multifrequency NQR [9], circularly polarized RF NQR [10] and others [11]. In addition to signal intensity increase, the detection probability can be improved by advanced signal processing. Here the main goal is to obtain the maximum detection probability from a given NQR response. Traditionally the principal NQR "signal processing" was noise reduction through averaging, which is very robust when inspecting an unknown response, but is very slow for TNT. When the response is known, better approaches exist. Particularly for TNT a very successful approach was developed

* Corresponding author.
E-mail address: alan.gregorovic@ijs.si (A. Gregorovič).

1090-7807/$ - see front matter © 2009 Elsevier Inc. All rights reserved.
doi:10.1016/j.jmr.2009.02.011

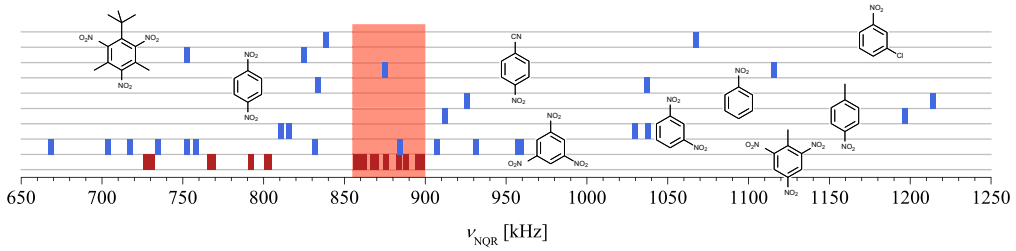

Fig. 1. NQR frequencies of some TNT related compounds at 77 K. The rows from top to bottom contain spectra for: *m*-chloronitrobenzene, 2,4,6-trinitro-1-*t*-butyl-3,5-dimethylbenzene, *p*-nitrobenzonitrile, nitrobenzene, *p*-nitrotoluene, *m*-dinitrobenzene, trinitrobenzene, and trinitrotoluene (orthorhombic and monoclinic). Only the ν_+ and ν_- frequencies are shown, while the $\nu_0 = \nu_+ - \nu_-$ frequencies are around 200 kHz. The shaded region shows the part of the spectrum that overlaps with the TNT ν_+ frequencies.

by Jakobsson et al. [12] for cases where the object temperature is only approximately known: the approximate maximum likelihood (AML) in time domain and the frequency selective AML (FSAML) in frequency domain. The later is slightly more robust under certain noise conditions.

In this paper, we combine the time domain AML detection technique and the SLSE pulse sequence to substantially improve the TNT detection probability. Treating both methods together gives us a deeper insight into the problem and thus the ability to fine tune the SLSE experiment. Working in time domain also allows us to use the full response of the SLSE sequence and not only its most intense part. Most of our experiments include signal enhancement with ^{1}H–^{14}N cross-polarization, however this is not essential and is used only to shorten the experimental time. We have conducted all experiments at a fixed temperature to remove one degree of freedom. In such a case the AML detector reduces to a matched filter detection. When the temperature is only approximately known the matched filter should be replaced by AML again.

2. Experimental setup

The experimental data has been obtained with a conventional home-built NQR spectrometer with the addition of a cross-polarizing unit, as described in Ref. [13].

2.1. ^{1}H–^{14}N cross-polarization

This unit consists of a $B_0 = 1.1$ T permanent magnet and a pressurized transfer tube, which is used to move the sample between the magnet and the excitation/detection coil. The sample is first placed in the magnetic field B_0. After 30 s the ^{1}H magnetization reaches a thermal equilibrium value and the sample is quickly moved to the NQR coil located 75 cm away, where the magnetic field is negligible. At some point during this transfer process the magnetic field decreases to such a value that the ^{1}H and ^{14}N energy levels equalized and some ^{1}H magnetization is transferred to ^{14}N. Finally, the ^{14}N magnetization of the TNT sample in the coil is $\sim 50\times$ larger than in a sample without the enhancement [7] suitable for any conventional NQR experiment. After the acquisition the sample is returned to the magnet and the cycle repeated.

2.2. Sample

The permanent magnet useful volume is enough for 70 g of TNT. We have used a commercial grade TNT, which in our case was a powder of 70% orthorhombic and 30% monoclinic phase. The 12 ν_+ TNT frequencies we observed lie in the range[4] 837 kHz $< \nu_+ <$ 871 kHz at room temperature and are listed in Table 1.

Table 1
TNT ^{14}N ν_+ NQR frequencies at $T = 300$ K for the 6 nonequivalent sites of the two crystallographic forms.

Orthorhombic TNT ν_+ (kHz)	Monoclinic TNT ν_+ (kHz)
837.5	836.5
841.5	841.7
846.3	843.5
848.0	847.7
861.0	858.1
868.2	869.7

2.3. Probe

The cylindrical excitation/detection coil had a diameter of 2 cm, was 7 cm long and was wound from a 0.8 mm copper wire. Its unloaded *Q*-factor was 120. The dead time of such a probe at TNT frequencies, ~ 500 μs, is unacceptably long for multipulse sequences and was lowered to less than 100 μs with a resistor parallel to the coil. The coil was then capacitively coupled to the excitation/detection circuit where the final *Q*-factor of the resonant circuit was 17 and the probe bandwidth 50 kHz [13]. The large bandwidth allowed us to detect all 12 TNT ν_+ lines without any retuning. The apparent 90° pulse length we used was 33 μs.

2.4. Spin-lock spin-echo pulse sequence

The signal is obtained by acquiring the NQR response while the sample is irradiated with the SLSE multipulse sequence [3], which is widely used nowadays to enhance the S/N ratio of ^{14}N NQR signals. The sequence (shown in Fig. 2) consist of a preparatory $90^\circ_{\pm y}$ pulse followed by a train of N_{seg} 90°_x pulses spaced t_c apart: $90^\circ_{\pm y} - (\tau - 90^\circ_x - \tau)_{N_{seg}}$, where $t_c = 2\tau + t_{90^\circ}$. In the nth segment, between pulses n and $n+1$, an NQR echo is formed with a peak at time t_n and its evolution is described by 12 components in TNT

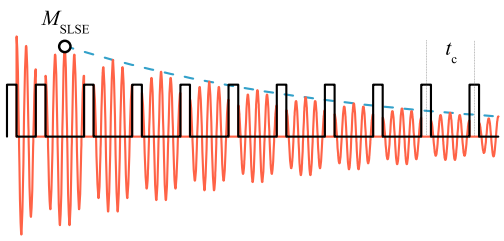

Fig. 2. NQR multipulse acquisition. The sample is exposed to a train of RF pulses (black) and the signal is induced between the pulses (red). The shape of the signal between two pulses has the form of an echo. (For interpretation of the references to color in this figure legend, the reader is referred to the web version of this paper.)

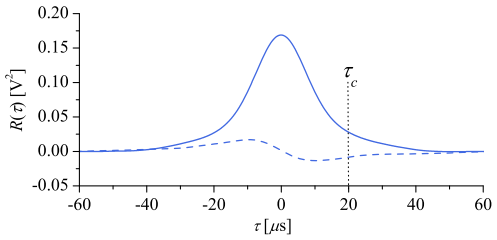

Fig. 3. Noise autocorrelation function $R(\tau)$. The solid line is for the in phase part and the dashed line for the out of phase part. The noise correlation time $\tau_c \sim 20$ μs.

$$s_n(t) = \sum_{k=1}^{12} \alpha_k \exp\left(i2\pi\nu_k(t - t_n) - \frac{|t - t_n|}{T^*_{2,k}} - \frac{t_n}{T_{2\mathrm{eff},k}} \right). \quad (1)$$

Here the kth component frequency is ν_k and α_k its real amplitude. The decay of the kth component echo is described by $T^*_{2,k}$, while the $T_{2\mathrm{eff},k}$ describes the echo attenuation across segments n. Some of these parameters depend only on the sample involved while others depend also on the particular pulse sequence parameters. Especially the frequencies ν_k (Table 1) are usually used as the primary signature of the sample. The other parameter which is independent of the experimental setup is $T^*_{2,k}$ and is almost k independent. The intensities α_k, depend on the pulse sequence parameters (mainly t_c) as well as on frequencies ν_k and can be evaluated exactly [13]. The last parameter $T_{2\mathrm{eff},k}$ seems to be quite k independent, but its increase with the decrease of t_c is well known. It also varies with other pulse sequence parameters [13] and needs further investigation.

Because the SLSE phase cycling has two steps where the response of the sequence with the first pulse 90°_{+y} is subtracted with the one where the first pulse is 90°_{-y}, the term "single-shot" throughout the article refers to one complete phase cycle.

2.5. Noise

Any acquisition inevitably contains some noise. The noise from external sources is dominant in remote detection, but can be successfully removed with gradiometric coils or additional antennas [14–16]. The internal noise however, mainly the coil's thermal noise, will remain, and its size is usually much bigger than the detected signal [2]. We are therefore dealing with thermal noise shaped by the probe and low-pass filters, e.g the resonant circuit itself and the anti-aliasing filter. In our experimental setup the probe was shielded, and the noise $w(t)$ characterized by its autocorrelation function $R(\tau) = \overline{w(t)w(t+\tau)}$ is shown in Fig. 3. This autocorrelation function is much different from the white noise autocorrelation function $R(\tau) = w^2_{\mathrm{rms}}\delta(\tau)$, where w_{rms} is the noise root mean square value, while $\delta(\tau)$ is the Dirac's delta function. In our case, the noise is clearly correlated with a correlation time $\tau_c \sim 20$ μs.

2.6. Signal

A well averaged ^{14}N NQR TNT signal obtained with the above setup is shown in Fig. 4. Here the excitation frequency was $\nu_{\mathrm{RF}} = 842$ kHz, the spacing between the pulses $t_c = 2$ ms, while the signal was averaged 1000 times. Each signal was enhanced by a factor of 50 with the cross-polarization technique [7]. In the spectrum of the second echo in Fig. 4c, 7 of the 12 TNT peaks are clearly seen. The two peaks at 868.2 and 869.7 kHz were not observed being too far from the excitation frequency, whereas the three remaining unresolved peaks overlap.

3. Matched filter detection

While it is easy to assign the spectrum in Fig. 4c to TNT after a comparison with the frequencies in Table 1, such assignment becomes unreliable in the presence of a large amount of noise. This problem can be solved with the use of a numerical procedure which we derive now.

The acquired signal in time domain $\mathbf{y}$ is a vector whose elements $y[i]$ are the N signal values sampled consecutively every Δt

$$\mathbf{y} = (y[1], y[2], \ldots, y[i], \ldots, y[N]). \quad (2)$$

We can write it as a sum of two parts: a noiseless part proportional to the TNT signal $\mathbf{s}$ (like the one shown in Fig. 4a) and noise $\mathbf{w}$

$$\mathbf{y} = \rho\mathbf{s} + \mathbf{w}. \quad (3)$$

Here the signal amplitude ρ ideally takes only two values: $\rho = 1$ when the TNT signal is present in $\mathbf{y}$, and $\rho = 0$ when it is absent. The basic algorithm to determine ρ from a noisy signal $\mathbf{y}$ is by finding the value of ρ which minimizes $\|\mathbf{y} - \rho\mathbf{s}\|^2$. It can be shown however[17], that whenever noise is correlated, that is when $R(\tau) \neq w^2_{\mathrm{rms}}\delta(\tau)$, a better solution is found by minimizing $\|\mathbf{y} - \rho\mathbf{s}\|^2_{\mathbf{R}}$, where $\mathbf{R} = \overline{\mathbf{w}\mathbf{w}^{\mathrm{T}}}$ is the noise covariance matrix ($R(\tau)$ defines $\mathbf{R}$ and vice versa). The two vector norms are defined as $\|\mathbf{a}\|^2 = \mathbf{a}^{\mathrm{T}}\mathbf{a}$ and $\|\mathbf{a}\|^2_{\mathbf{P}} = \mathbf{a}^{\mathrm{T}}\mathbf{P}^{-1}\mathbf{a}$. Minimization of $\|\mathbf{y} - \rho\mathbf{s}\|^2_{\mathbf{R}}$ is also the starting point in the derivation of the AML detector[12] and many other signal processing techniques. The above minimization yields the most likely amplitude of the reference signal $\mathbf{s}$ in the acquired noisy signal $\mathbf{y}$

$$\rho_{\mathrm{mf}}(\mathbf{y}) = \frac{\mathbf{s}^{\mathrm{T}}\mathbf{R}^{-1}\mathbf{y}}{\mathbf{s}^{\mathrm{T}}\mathbf{R}^{-1}\mathbf{s}}. \quad (4)$$

which is then used for comparing against a predetermined threshold value to give a true/false answer. The Eq. (4) is one of the many forms used to express the matched filter (mf) or optimal detector [18,19].

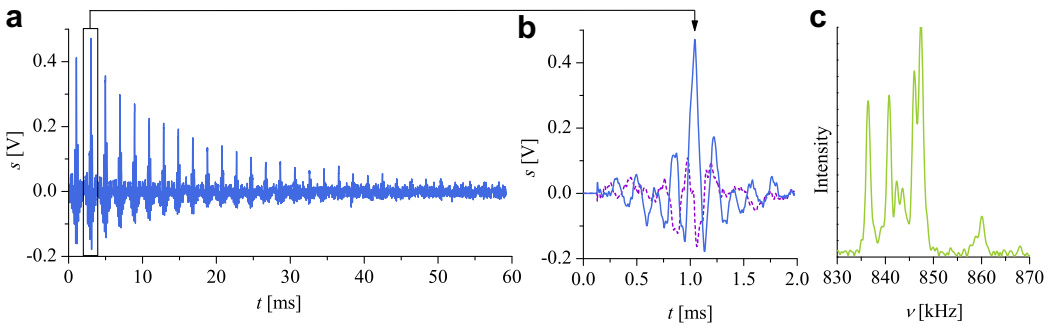

Fig. 4. TNT ^{14}N NQR signal acquired with a SLSE multipulse sequence at $\nu_{\mathrm{RF}} = 842$ kHz and $t_c = 2$ ms: (a) full acquisition with all segments, (b) second echo only, with the in phase signal (solid blue) and out of phase signal (dashed violet) and (c) absorption spectrum of the second echo showing characteristic TNT ^{14}N NQR frequencies from Table 1. From the echo decays in a) we find $T_{2\mathrm{eff}} \approx 17$ ms. (For interpretation of the references to color in this figure legend, the reader is referred to the web version of this paper.)

The vector **y** contains signal acquired in all segments, so that its size N can be a large number of the order of 10^5 and the size of the matrix $\mathbf{R}, N^2$, is then unmanageable. However, the noise correlation length $\tau_c \sim 20\,\mu s$ (see Fig. 3) is substantially shorter than the acquisition length $N\Delta t \sim 150$ ms and also the segment length t_c, therefore most values in the matrix **R** will be zero. With this in mind, we can replace the true matrix **R** by its approximation, which assumes that the noise in different segments is fully uncorrelated. This is certainly true for two nonconsecutive segments due to $\tau_c \ll t_c$, however, the noise in two consecutive segments is correlated at the boundary between them. In our case, this is not a serious issue because τ_c is much shorter than the experimental dead time (~ 100 μs). With the above considerations **R** becomes a block diagonal matrix

$$\mathbf{R} = \begin{pmatrix} \widetilde{\mathbf{R}} & 0 & \cdots & 0 \\ 0 & \widetilde{\mathbf{R}} & & \vdots \\ \vdots & & \ddots & 0 \\ 0 & \cdots & 0 & \widetilde{\mathbf{R}} \end{pmatrix} \tag{5}$$

where each block is the single segment covariance matrix $\widetilde{\mathbf{R}}$. We will similarly split also the vectors **y**, **s**, and **w** into N_{seg} vectors $\mathbf{y}_n, \mathbf{s}_n$, and $\mathbf{w}_n$ containing only elements from the nth segment, so that the covariance matrix $\widetilde{\mathbf{R}}$ is written as

$$\widetilde{\mathbf{R}} = \overline{\mathbf{w}_n \mathbf{w}_n^{\mathrm{T}}}, \tag{6}$$

but is n independent. The matched filter amplitude from Eq. (4) is then written as

$$\rho_{\mathrm{mf}}(\mathbf{y}) = \frac{\sum_n \mathbf{s}_n^{\mathrm{T}} \widetilde{\mathbf{R}}^{-1} \mathbf{y}_n}{\sum_n \mathbf{s}_n^{\mathrm{T}} \widetilde{\mathbf{R}}^{-1} \mathbf{s}_n}. \tag{7}$$

For a set of identical single-shot acquisitions, we obtain a set of different vectors **y** due to the presence of noise and correspondingly, a set of different amplitudes $\rho_{\mathrm{mf}}(\mathbf{y})$. The amplitudes average value is $\bar{\rho} = \rho_{\mathrm{mf}}(\mathbf{s}) = 1$ when the TNT signal is present in **y** and $\bar{\rho} = 0$ in its absence. On the other hand, the amplitudes standard deviation

$$\sigma_{\mathrm{mf}} = \sqrt{\overline{(\rho_{\mathrm{mf}}(\mathbf{y}) - \bar{\rho})^2}} = \frac{1}{\sqrt{\sum_n \mathbf{s}_n^{\mathrm{T}} \widetilde{\mathbf{R}}^{-1} \mathbf{s}_n}} \tag{8}$$

is same for both cases ($\bar{\rho}$ independent) and is a measure of the detector's single-shot detection capabilities. We expect a good single-shot detection only when $\sigma_{\mathrm{mf}} \ll 1$, i.e. when the scattering is much smaller than the difference between the two average values. Another common way of characterizing the detector's efficiency is its single-shot signal-to-noise ratio

$$S/N = \frac{(\rho_{\mathrm{mf}}(\mathbf{s}))^2}{\sigma_{\mathrm{mf}}^2} = \sum_n \mathbf{s}_n^{\mathrm{T}} \widetilde{\mathbf{R}}^{-1} \mathbf{s}_n. \tag{9}$$

We owe another explanation before proceeding. In the above derivation the vectors **y**, **s** and **w** are assumed to be real, whereas the NQR signal $s(t)$ and noise $w(t)$ are usually expressed as complex quantities (in-phase and out-of-phase components after demodulation). But, because the pursued amplitude ρ is real, we build the corresponding vectors **y**, **s**, and **w** as real vectors. This can be done in several equivalent ways, e.g. by alternating the real and imaginary part of the signal $\mathbf{y} = [\ldots, y_{\mathrm{re}}(m\Delta t), y_{\mathrm{im}}(m\Delta t), \ldots]$.

3.1. White noise approximation

It is here insightful to deal first with white noise, by assuming $R(\tau) = w_{\mathrm{rms}}^2 \delta(\tau)$. The corresponding covariance matrix (Eq. (6)) becomes diagonal

$$\widetilde{\mathbf{R}} = w_{\mathrm{rms}}^2 \mathbf{I} \tag{10}$$

and the matched filter amplitude $\rho_{\mathrm{mf}}(\mathbf{y})$ simplifies to the well known cross-correlation

$$\rho_{\mathrm{cc}}(\mathbf{y}) = \frac{\mathbf{s}^T \mathbf{y}}{\mathbf{s}^T \mathbf{s}}, \tag{11}$$

which estimates the similarity of two signals. For a set of identical single-shot acquisitions the cross-correlation amplitudes $\rho_{\mathrm{cc}}(\mathbf{y})$ will again be scattered around two values: $\bar{\rho} = \rho_{\mathrm{cc}}(\mathbf{s}) = 1$ and $\bar{\rho} = 0$, whereas the corresponding standard deviation is found by inserting Eq. (10) in Eq. (8) as

$$\sigma_{\mathrm{white}} = \frac{w_{\mathrm{rms}}}{\sqrt{\mathbf{s}^{\mathrm{T}} \mathbf{s}}} \tag{12}$$

This is now a very simple expression and one can draw a rather obvious conclusion. In order to minimize σ_{white} and thus increase the robustness of detection, one has either to: (i) decrease noise w_{rms} or (ii) increase signal $\mathbf{s}^{\mathrm{T}}\mathbf{s}$. The first option makes sense only to certain extent, as w_{rms} value for a single-shot detection is determined by the detector bandwidth and temperature. The bandwidth is usually chosen so that the whole signal is observed, and its reduction reduces $\mathbf{s}^{\mathrm{T}}\mathbf{s}$ as well. However, the probe bandwidth also determines the detector Q-factor, which will increase upon bandwidth decrease, and consequently increase $\mathbf{s}^{\mathrm{T}}\mathbf{s}$. The overall effect of bandwidth change is an interplay of the two effects, and not further discussed here. Noise w_{rms} can be decreased also by lowering the detector's temperature, e.g. by immersion in liquid nitrogen, *but this option requires specialized hardware*. On the other hand, there are at least two ways of increasing $\mathbf{s}^{\mathrm{T}}\mathbf{s}$ easily: (i) acquiring more points with faster sampling and (ii) acquiring more echoes by reducing SLSE pulse spacings. Both options seem interesting also from the remote detection point of view and we explore them now.

3.2. Approximation for colored noise

Instead of repeating the acquisition at every possible combination of Δt and t_c we use the acquisition **s** from Fig. 4a to numerically obtain the signal **s′** which would be obtained with other values of Δt and t_c. This procedure is not equivalent to a real experiment, however, it allows us to study the Δt and t_c effects independently from the well known $T_{2\mathrm{eff}}$ and α_k dependence on t_c [13]. On the other hand, the noise autocorrelation function $R(\tau)$ is independent of Δt and t_c so that the corresponding matrix $\widetilde{\mathbf{R}}$ is easily determined from $R(\tau)$ in Fig. 3.

The dependence of σ_{mf} on the sampling interval Δt is obtained with the help of decimation. The signal **s** was acquired with a short sampling interval $\Delta t = 3.6$ μs. Therefore, **s′** sampled every

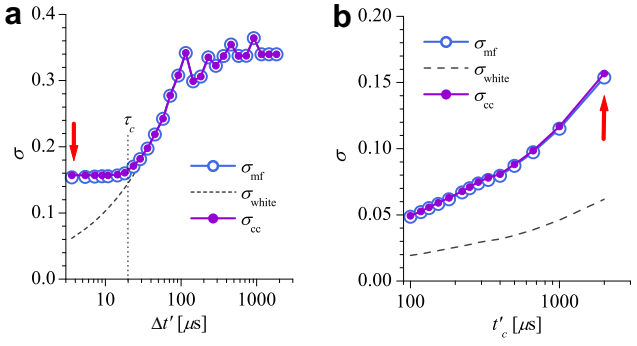

Fig. 5. Standard deviations $\sigma_{\mathrm{mf}}, \sigma_{\mathrm{cc}}$, and σ_{white} dependences on (a) sampling interval and (b) pulse spacing, as found by a numeric procedure from a real signal (denoted by a red arrow).

$\Delta t' = m\Delta t$ is easily obtained from **s** by retaining only its every mth element. The standard deviation σ_{mf} is then found by replacing **s** with **s′** in Eq. (8) together with an appropriate $\widetilde{\mathbf{R}}$. The results for various $\Delta t'$ are shown in Fig. 5a. As it is expected σ_{mf} decreases with decreasing $\Delta t'$ as long as $\Delta t'$ is longer than the noise correlation time τ_c. In this region the acquired noise appears white so that $\sigma_{mf} = \sigma_{white}$ and one could easily use cross-correlation $\rho_{cc}(\mathbf{y})$ instead of the matched filter $\rho_{mf}(\mathbf{y})$, the former being much easier to calculate than the later. Decreasing $\Delta t'$ below τ_c brings no further reduction of σ_{mf}. In this regime the acquired noise is colored (correlated) due to the applied filters, although the noise at its origin (thermal noise) is white. Because the signal and noise are subjected to the same filters, no further information is obtained when $\Delta t'$ is decreased below τ_c so σ_{mf} stays the same. We should remark here, that the matched filter average value $\bar{\rho}_{mf} = 1$ is independent of $\Delta t'$ by definition.

It is less straightforward to determine the influence of pulse spacing t_c on σ_{mf}. In this case the signal **s′** at shorter t_c' is found by a suitable reduction and interpolation of the signal **s**. For example, when t_c is halved, the number of segments is doubled. In every new segment an echo at the center appears, so that we have twice as many echoes as before. The new odd echoes are obtained from the old echoes simply by dropping their first and last quarter (the region around the echo peak is kept), whereas the new even echoes are obtained by averaging their odd neighbors. This procedure is easily generalized to obtain the signal **s′** at any $t_c' < t_c$ and the results for $100\,\mu s < t_c' < 2\,ms$ based on a signal with $t_c = 2\,ms$ is shown in Fig. 5b. The results are surprising. When t_c' decreases, σ_{mf} monotonically decreases as well. The smallest value of σ_{mf} is thus found at $t_c' = 100\,\mu s$, and is more than 3 times smaller than σ_{mf} at $t_c = 2$ ms. Such an increase of sensitivity is translated to a significant ~ 10 dB S/N increase. The effect is not difficult to explain however: when $t_c > 6T_2^*$ the main contribution to $\sum_n \mathbf{s}_n^T \widetilde{\mathbf{R}}^{-1} \mathbf{s}_n$ comes from magnetization in the segments central region, around the echo peak, whereas segment extremities contain little magnetization; the magnetization either starts to buildup from noise or has already fully decayed below the noise level. When t_c is reduced so that $t_c < 6T_2^*$, the magnetization has no time to fully decay but rather decays to a finite value. Similarly, also the buildup starts from a finite value rather than from noise. This magnetization at extremities increases with decreasing t_c, and its contribution to $\sum_n \mathbf{s}_n^T \widetilde{\mathbf{R}}^{-1} \mathbf{s}_n$ and thus σ_{mf} becomes increasingly more important.

The values of $\sigma_{mf} \ll 1$ indicate a very high S/N. In fact, in the above example the signal single-shot S/N is 16.5 dB and such a large value is due to the 50× signal enhancement with ^{1}H-^{14}N cross-polarization technique. Here, the presence of TNT in **y** is easily determined also with an inspection "by eye". This single-shot S/N ratio should not be confused with the 30 dB higher S/N ratio of the experiment in Fig. 4, where 1000 averages have been done.

It is often the case that due to its simplicity cross-correlation $\rho_{cc}(\mathbf{y})$ is implemented rather than the matched filter $\rho_{mf}(\mathbf{y})$ even if the noise is colored (correlated). Under such conditions the amplitudes $\rho_{cc}(\mathbf{y})$ average value is still $\bar{\rho} = 1$, when TNT is present, and $\bar{\rho} = 0$, when it is not, but the standard deviation would be erroneously described by σ_{white} in Eq. (12) as shown in Fig. 5. The correct value for $\rho_{cc}(\mathbf{y})$ standard deviation when $\widetilde{\mathbf{R}} \neq w_{RMS}^2 \mathbf{I}$ is easy derived as

$$\sigma_{cc} = \frac{\sqrt{\sum_n \mathbf{s}_n^T \widetilde{\mathbf{R}} \mathbf{s}_n}}{\sum_n \mathbf{s}_n^T \mathbf{s}_n} \tag{13}$$

and is much larger than σ_{white}. Also, the value of σ_{cc} should always be larger than σ_{mf}, because $\rho_{mf}(\mathbf{y})$ is derived by properly considering the noise correlation while $\rho_{cc}(\mathbf{y})$ is not. However, we find a very small difference between σ_{mf} and σ_{cc} which hardly justifies the use of the matched filter instead of the cross-correlation as shown in Fig. 5. This is probably due to the fact that at the origin the thermal noise is white but later, the noise as well as the NQR signal are both subjected to identical filters.

4. Experimental results and discussion

To check the conclusions in Section 3.2 we repeated the experiment in Fig. 4 with a very short $t_c = 540\,\mu s$. The response averaged 2000 times is shown in Fig. 6a. It is immediately evident, that we have acquired much more magnetization than when a longer t_c was used. Moreover, the relaxation time $T_{2eff} \approx 43$ ms is now considerably longer than $T_{2eff} \approx 17$ ms at $t_c = 2$ ms and additionally contributes to the acquired magnetization. In Fig. 6b, only the second echo is shown, with its Fourier transform in Fig. 6c. The spectral resolution is now limited by a short t_c and is ~ 2 kHz. The spectrum is severely smeared so that its comparison with the frequencies in Table 1 is nontrivial, and a reliable attribution to TNT difficult.

In contrast, the corresponding single-shot standard deviation σ_{mf}, obtained by inserting the new response **s** (from Fig. 6a) in Eq. (8) is very small indicating a good detector. We find an encouraging value of $\sigma_{mf} = 0.03$ or a $S/N = 30.5$ dB, whereas the values for the acquisition with $t_c = 2$ ms are $\sigma_{mf} = 0.26$ and $S/N = 16.5$ dB. Thus simply by reducing t_c we have increased S/N by 14 dB. Some of this enhancement is due to the longer T_{2eff}, whereas the main part is due to the increased number of observed echoes.

Of course, the $S/N = 16.5$ dB is already sufficient for a reliable detection, and at first its increase to 30.5 dB does not seem necessary. However, in all the above experiments we have used the 50× signal enhancement by cross-polarization which increases S/N by 34 dB. If this enhancement is removed (e.g. because such enhancement values are almost impossible to obtain outside the

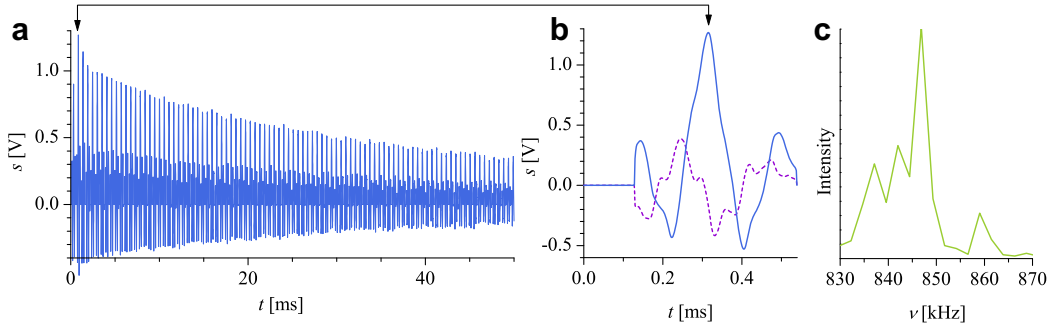

Fig. 6. TNT ^{14}N NQR signal acquired with a SLSE multipulse sequence at $\nu_{RF} = 842$ kHz and a very short pulse spacing $t_c = 540\,\mu s$: (a) first 100 echoes, (b) second echo only, with the in phase signal (solid blue) and out of phase signal (dashed violet) and (c) absorption spectrum of the second echo. The individual lines are here less clearly resolved than in Fig. 4c. From the echoes in a) we determine $T_{2eff} \approx 43$ ms.

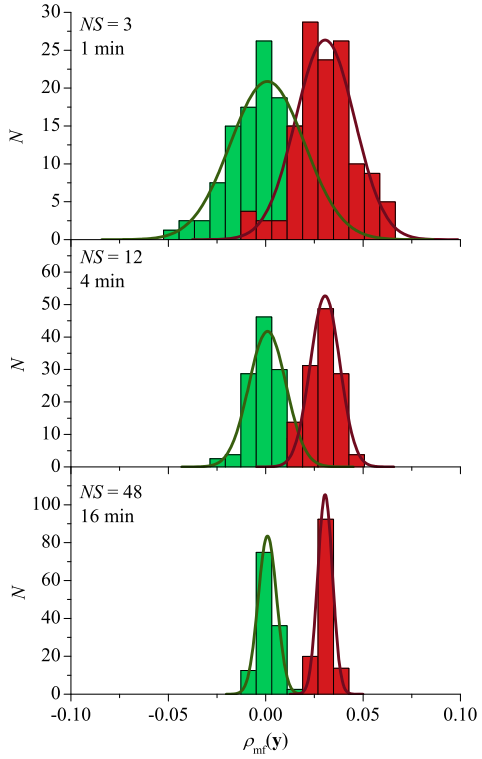

Fig. 7. TNT signal intensities ρ_{mf} distributions of low-resolution NQR signals with three different number of averages (*NS*): 100 experiments with empty detector (green, lighter bars) and 100 experiments with the presence of TNT (red, darker bars) but without signal enhancement. The averages used in each setup were: 3 (top), 12 (middle), 48 (bottom). The solid curves represent predicted distributions from the signal in Fig. 6. (For interpretation of the references to color in this figure legend, the reader is referred to the web version of this paper.)

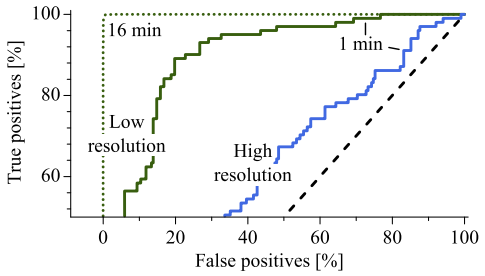

Fig. 8. Comparison of the ROC curves for (i) high-resolution NQR signals in 1 min (blue curve) (ii) low-resolution signals in 1 min (solid green) and (iii) low-resolution signals in 16 min (dotted green). The ROC curve is here a parametric function of a threshold value (not shown) and a histogram (Fig. 7). For each threshold value we count the number of false and true positives in the histogram, so that these values define the ROC curve's *x* and *y* coordinate. The aim of any detector is to get as close as possible to the upper left corner of the graph. (For interpretation of the references to color in this figure legend, the reader is referred to the web version of this paper.)

laboratory), a $t_c = 540\,\mu s$ detection would only result in $S/N \sim -3.5$ dB. This value is now smaller than the threshold value of 10 dB, usually required for an acceptable rate of false alarms [2], but nevertheless a good starting point. For example the value of 10 dB is obtained, if the enhancement is not completely removed, but rather reduced to 4.7×, obtained with a small magnetic field of ∼ 120 mT. Or, instead of requiring a single-shot detection, we allow some time for averaging. Only 22 averages without any enhancement are now needed to obtain a $S/N = 10$ dB. Both options seem a reasonable solution for remote detection.

4.1. Detection with pure NQR

To check the detectability of the pure ^{14}N NQR TNT signal, that is without the use of any signal enhancement, we have made a series of 100 experiments, a set of 100 **y** vectors, with the $t_c = 540\,\mu s$ as in Fig. 6. Here, the expected signal exactly retains its form but is 50× smaller than the reference signal from Fig. 6a. Because the signal is now so minute and not seen "by eye", also 100 responses of the empty coil have been measured for comparison. In both cases, the signal amplitude is determined with $\rho_{mf}(\mathbf{y})$ using **s** from Fig. 6a. We expect now an $\bar{\rho} = 1/50$ when TNT is in the coil, and $\bar{\rho} = 0$ when the coil is empty. The single-shot standard deviation around these values is however unchanged as can be verified by Eq. (8). Thus, the expected $\sigma_{mf} = 0.03$ is now big compared to the difference between the two average values $\Delta\bar{\rho} = 1/50$ and we decided to look at signals from few small number of averages.

The histograms of the 100 amplitudes $\rho_{mf}(\mathbf{y})$ are shown in Fig. 7 for three representative number of averages (*NS*). In Fig. 7a $NS = 3$ with a total acquisition time of 1 min. Here the individual TNT response (not shown) bears no resemblance with the one in Fig. 6 since it is now totally dominated by noise. But the $\rho_{mf}(\mathbf{y})$ distributions already show some clues. The red (darker) columns in Fig. 7a represent the distribution of $\rho_{mf}(\mathbf{y})$ with the presence of TNT in the coil, whereas the green (lighter) columns show only the empty coil response. The centers of gravity of the two distributions clearly do not coincide. When the coil is empty, the distribution is centered at $\bar{\rho} = 0$ as expected, when the coil is filled with TNT, the distribution center moves to $\bar{\rho} = 0.03$. This value is slightly larger than the expected 1/50, presumably because a non-optimal polarization transfer between ^{1}H and ^{14}N (the gain is smaller than 50). The width of the distributions is here comparable to the separation between them so that the averaging time of 1 min results only in S/N = 4.9 dB, not enough for a useful detection. With averaging, the two distributions centers of gravity do not change, while their widths are proportional to $1/\sqrt{NS}$. In Fig. 7b we show the distribution of 100 amplitudes $\rho_{mf}(\mathbf{y})$ determined after the acquisitions have been averaged 12 times, that is for 4 min. As expected, the result is now much better with a S/N = 11 dB. If the averaging time is further extended to 16 min with 48 averages, the detection becomes almost perfect as shown in Fig. 7c, with a $S/N = 17$ dB. For an easier comparison with other detectors, the results of Fig. 7 are shown also with the receiver operating characteristic (ROC) curve in Fig. 8.

Of course, the detection time of 4 min for the sample in the coil does not seem promising at first. In remote detection the sample would be located a few cm away from the coil and significantly more averages would be needed for a similar level of reliability. We should not forget however, that we have used a realistic anti-personnel landmine quantity of TNT (70 g) at room temperature, whereas in a typical study [4] a large sample (> 400 g) was cooled to 77 K to obtain an acceptable *S*/*N*.

4.2. Q-factor optimization

In the present setup a passive coil-ringdown suppression circuit was used. This is an effective but very primitive realization and calls for an improvement. We are in a process to build and active coil-ringdown suppression circuit [20], with same or shorter dead time, but larger *Q*. We believe that for TNT an optimal bandwidth is around 15 kHz, so that the target resonant circuit is $Q \sim 56$. Such a bandwidth would be enough to capture all TNT lines in the range 837–852 kHz, with negligible loss in total intensity. The foreseen *S*/*N* increase compared to the present setup is 5.2 dB, just about the value required for a useful detection in 1 min. A $Q \gg 56$ might not bring a much better result, as the narrow bandwidth will

decrease the number of detected lines, but this needs to be checked experimentally [21,22]. Another limiting factor of a high-Q probe is its temperature stability. Whereas in our configuration with 50 kHz bandwidth probe the magnitude of TNT intensity is almost T independent in a region of interest $-10^\circ < T < 40^\circ$, an extremely narrowband detector focused on a single TNT line might see considerable variation of the intensity, as a consequence of the focused line moving in and out of the observation window with the change in the object's temperature.

4.3. Spurious signal rejection

Looking back at Fig. 6c it seems that the NQR primary advantage over competing techniques for explosive detection, its unequivocal signature, has been lost because of resulting reduction due to the short acquisition time. The spectrum losses many of its characteristic features when short t_c is used, and the prospect of further t_c reduction to additionally increase the S/N will make things even worse. However, a resolution where all TNT lines coalesce might still be good enough to discriminate TNT from other materials. In Fig. 1 we have collected [23] the NQR frequencies of some nitrobenzenes with similar molecular structure as TNT. As it is evident, the region is ~ 600 kHz wide and the overlap with the TNT frequencies, as chosen in this experiment, is minimal. Of course many more compounds with NO_2 groups exist and are not shown. Their NQR frequencies will very likely be in the same frequency range, and possibly overlap with the TNT frequencies. If this happens to be the case or problem, there is a secondary TNT characteristic parameter, $T_{2\mathrm{eff}}$. While the frequencies are influenced by the ^{14}N averaged local environment, roughly defined by the $-NO_2$ group, the relaxation times are determined by dynamic phenomena, mainly the motions of small molecular fragments, e.g. $-CH_3$ and other $-NO_2$ groups. The specific combination of them will compensate for the reduced resolution. As an example, at the same experimental conditions in TNT $T_{2\mathrm{eff}} \sim 43$ ms, while in paranitrotoluene (1 nitro group instead of 3) $T_{2\mathrm{eff}} = 400$ ms, a distinguishable change [13].

A low resolution response has another advantage in the case of TNT. The two polymorphs, orthorhombic and monoclinic, have overlapping NQR frequencies. In the low resolution response they become indistinguishable and remove another unknown parameter, the sample relative composition.

4.4. Obtaining a realistic reference signal for remote detection

The determination of the amplitudes ρ with a matched filter requires precise knowledge of the reference signal $\mathbf{s}$ and the noise autocorrelation function $R(\tau)$, whereas their determination with cross-correlation requires only the signal. Obtaining the noise autocorrelation function is in principle easy. The same is not true for the reference signal. In fact, obtaining a noiseless reference signal is a very tough condition to fulfill for TNT. Its low intrinsic S/N makes this impossible without some kind of signal enhancement. For example, the signal in Fig. 6a was obtained with 2000 averages and with the 50× enhancement. A pure NQR (no enhancement) experiment would take 2500 times more averages to obtain a similar S/N meaning 5 million averages, or a prohibitively long time.

In the field an additional problem is that the target from which we need to obtain the reference signal is hidden and its temperature unknown. The solution to this problem is signal modeling through Eq. (1) at various T. Because the NQR signal dependence on T is nonlinear, the matched filter approach becomes unsuitable and needs to be replaced. An example of a very efficient algorithm which takes these nonlinearities into account is the ETAML algorithm[24]. Because both algorithms minimize the same quantity, the performance increase will be similar. There are other parameters important for efficient signal modeling. Some of these parameters are known (ν_k), some are easy to obtain ($T^*_{2,k}$ and α_k), while some are more difficult to obtain ($T_{2\mathrm{eff},k}$) and need additional investigation. In particular $T_{2\mathrm{eff},k}$ dependence on t_c, T and RF field strength should be well understood.

5. Conclusions

We use the matched filter to determine the presence of TNT signal in the ^{14}N NQR SLSE response.

We derive a theoretical expression for the detection S/N, and use it to optimize the SLSE pulse sequence parameters. We find that the easiest way to improve the detection performance is by determining the optimal pulse spacing t_c and sampling interval Δt. Then, based on a reference TNT SLSE signal, we numerically investigate the S/N dependence on t_c and Δt. Contrary to intuition, the S/N steadily increases when t_c decreases, so that a low spectral resolution acquisition becomes much more advantageous than a high resolution one. In contrast, the increase of S/N upon the decrease of Δt reaches its terminal value when Δt equals the noise correlation time τ_c. We also assess the detection capability of the SLSE matched filter with optimized parameters on TNT with pure NQR without any signal enhancement. Our conclusions are not limited to the SLSE pulse sequence, but are valid for a wide range of newer multipulse sequences which create the spin-lock effect. We envisage that multipulse sequences with short pulse spacings can significantly shorten the time for TNT detection or increase the reliability of detection.

References

[1] A.N. Garroway, M.L. Buess, J.B. Miller, J.B. Suits, A.D. Hibbs, G.A. Barrall, R. Matthews, L.J. Burnett, IEEE Trans. Geosci. Rem. Sens. 39 (6) (2001) 1108.
[2] A.D. Hibbs, Alternatives for Landmine Detection, RAND, Santa Monica (CA), USA, 2003, Ch. Nuclear quadrupole resonance, p. 170. Available from: <http://www.rand.org/pubs/monograph_reports/MR1608/MR160 8.appj.pdf>.
[3] R.A. Marino, S.M. Klainer, J. Chem. Phys. 67 (7) (1977) 3388–3389.
[4] R.A. Marino, R.F. Connors, J. Mol. Struc. 111 (1983) 323.
[5] R. Blinc, J. Seliger, D. Arčon, P. Cevc, V. Žagar, Phys. Stat. Sol. (b) Applied Research 180 (2) (2000) 541.
[6] M. Nolte, A. Privalov, J. Altmann, V. Anferov, F. Fujara, J. Phys. D: Appl. Phys. 35 (9) (2002) 939.
[7] J. Lužnik, J. Pirnat, V. Jazbinšek, T. Apih, A. Gregorovič, R. Blinc, J. Seliger, Z. Trontelj, Appl. Phys. Lett. 89 (2006) 123509.
[8] J. Lužnik, J. Pirnat, V. Jazbinšek, T. Apih, R. Blinc, J. Seliger, Z. Trontelj, J. App. Phys. 102 (8) (2007).
[9] K.L. Sauer, B.H. Suits, A.N. Garroway, J.B. Miller, Chem. Phys. Lett. 342 (3-4) (2001) 362.
[10] J.B. Miller, B.H. Suits, A.N. Garroway, J. Mag. Res. 151 (2) (2001) 228.
[11] D.W. Prescott, O. Olmedo, S. Soon, K.L. Sauer, J. Chem. Phys. 126 (20) (2007) 204504.
[12] A. Jakobsson, M. Mossberg, M.D. Rowe, J.A.S. Smith, IEEE Trans. Geosci. Rem. Sens. 43 (11) (2005) 2659.
[13] A. Gregorovič, T. Apih, J. Chem. Phys. 129 (2008) 214504.
[14] A.S. Peshkovsky, C.J. Cattena, L.M. Cerioni, T.M. Osan, J.G. Forguez, W.J. Peresson, D.J. Pusiol, J. Mag. Res. 194 (2) (2008) 222.
[15] B.H. Suits, A.N. Garroway, J. Appl. Phys. 94 (6) (2003).
[16] B.H. Suits, A.N. Garroway, J.B. Miller, J. Mag. Res. 131 (1) (1998) 154.
[17] P. Stoica, R. Moses, Spectral Analysis of Signals, Prentice-Hall, Upper Saddle River, NY, 2005.
[18] G.L. Turin, IRE Trans. Inform. Theory 6 (3) (1960) 311.
[19] Wikipedia, Matched filter—Wikipedia, The Free Encyclopedia, 2008. Available from: <http://en.wikipedia.org/w/index.php?title=Matched_filter&oldid=249919334>.
[20] A.S. Peshkovsky, J. Forguez, L. Cerioni, D.J. Pusiol, J. Mag. Res. 177 (1) (2005) 67.
[21] B.H. Suits, A.N. Garroway, J.B. Miller, J. Mag. Res. 132 (1) (1998) 54.
[22] J.B. Miller, B.H. Suits, A.N. Garroway, M.A. Hepp, Conc. Mag. Res. 12 (3) (2000) 125.
[23] R.A. Marino, R.F. Connors, L. Leonard, Nitrogen-14 NQR study of energetic materials, Tech. Rep. 15556.4-PH, Block Engineering, Cambridge, MA 02139, September 1982.
[24] S.D. Somasundaram, A. Jakobsson, J.A.S. Smith, K. Althoefer, IEEE Trans. Geosci. Rem. Sens. 45 (4) (2007) 925.